Neural plate pre-patterning enables specification of intermediate neural progenitors in the spinal cord

Authors:
Sandy Nandagopal[1, *], Anna Cha[1], Bill Z. Jia[1], Hongyu Liao[1], Caroline Comenho[1], Galit Lahav[1], Daniel E. Wagner[2], Tony Y-C Tsai[3], Sean G. Megason[1, *]

Affiliations:
[1] Department of Systems Biology, Blavatnik Institute at Harvard Medical School, Boston, MA 02115
[2] Eli and Edythe Broad Center for Regeneration Medicine and Stem Cell Research and Department of Obstetrics, Gynecology and Reproductive Science, UCSF, San Francisco, CA 94143 USA
[3] Department of Developmental Biology, Washington University School of Medicine, St. Louis, Missouri, USA

[*] Correspondence: sandy.nandagopal@gmail.com; sean_megason@hms.harvard.edu

Summary
Dorsal-ventral patterning of neural progenitors in the posterior neural tube, which gives rise to the spinal cord, has served as a model system to understand how extracellular signals organize developing tissues. While previous work has shown that signaling gradients diversify progenitor fates at the dorsal and ventral ends of the tissue, the basis of fate specification in intermediate regions has remained unclear. Here we use zebrafish to investigate the neural plate, which precedes neural tube formation, and show that its pre-patterning by a distinct signaling environment enables intermediate fate specification. Systematic spatial analysis of transcription factor (TF) expression and signaling activity using a reference-based mapping approach shows that the neural plate is partitioned into a striking complexity of TF co-expression states that, in part, correspond to the activity of gastrulation signals such as FGF and Wnt that persist through axis extension. Using *in toto* analysis of cellular movement combined with fate mapping, we find that *dbx1b*-expressing intermediate progenitors (p0) originate from a neural-plate specific state characterized by transient co-expression of the TFs *pax3a*, *olig4* and *her3*. Finally, we show that this state is defined by Wnt signaling in the posterior neural plate and that ectopic Wnt activation within *pax3a/olig4*+ cells is sufficient to promote *dbx1b* expression. Our data broadly support a model in which neural progenitor specification occurs through the sequential use of multiple signals to progressively diversify the neural tissue as it develops. This has implications for *in vitro* differentiation of spinal cord cell types and for understanding signal-based patterning in other developmental contexts.

Introduction
The development of functional tissues and organs relies on the proper specification and organization of diverse cell types. Extracellular signals play critical roles in orchestrating this process, providing cells with timely, position-dependent cues to enable contextual cell fate

specification. A central goal in developmental biology is to understand how signals are utilized to pattern tissues in different contexts.

Work across developmental systems has revealed various signal-based patterning strategies, such as the use of long-range morphogen gradients that can provide positional information[1,2], local signaling interactions that can generate fine-grained patterns[3], and reaction-diffusion mechanisms that can self-organize complex patterns[4]. Many of these mechanisms are currently best understood in the context of a single signal operating in a relatively static tissue context, though there have been efforts to extend them to include the effects of temporal changes in signal perception, for example due to tissue growth[5–7].

Tissues often undergo changes in morphology and cellular arrangements concomitantly with fate specification[8,9]. This could alter the signaling environment, through changes in the levels as well as the types of signals that cells experience. Features of dynamic signaling environments present distinct challenges and opportunities for cell fate specification. On the one hand, fluctuating signal levels could blur positional information, reducing the precision of patterning, and necessitating additional error-correction mechanisms such as cell sorting[9–11]. On the other hand, time-varying features of signals, signaling relays (where cells are exposed to a sequence of different signals), and differential signal perception among cells due to cellular rearrangements, could all provide additional information that can be utilized for cell fate decision-making[12–16]. Therefore, dynamic tissue contexts might utilize unique patterning mechanisms but these are less well understood.

Vertebrate spinal cord development provides a good system to investigate the role of a dynamic signaling environment on patterning. The spinal cord develops from the posterior neural tube, which is patterned into 11 distinct neural progenitor domains along the dorsal-ventral (DV) axis. The neural tube, in turn, arises from the neural plate, through extensive morphogenetic movements that serve to extend the tube in step with elongation of the embryonic axis[17]. Previous work has shown that the signaling molecules Sonic hedgehog (Shh) and Bone Morphogenetic Protein (BMP) form signaling gradients from the ventral and dorsal ends of the neural tube, respectively, that help specify progenitor fates[18–21]. However, these signals do not appear to provide the information required for the ordered specification of fates in the intermediate positions of the DV axis. Intermediate p0 and p1 progenitors do not require Shh signaling for their specification in zebrafish[22–24], while in mouse Shh signaling plays a permissive role but is not strictly required for their specification or arrangement[25,26]. BMP signaling is also dispensable for the specification of intermediate neural progenitors, though it might impact their differentiation[18–20,27].

Prior to joining the neural tube, cells experience a distinct signaling environment in the neural plate. Cells in the posterior neural plate are located proximally to sources of signals such as FGF and Wnt[28–30]. As the embryonic axis extends, cells move away from posterior signals and begin to experience retinoic acid (RA) and Notch signaling[28,31,32]. Neural plate signaling has primarily been linked to regulating competence for neural specification[30,33,34] or neurogenesis[31,32,35]. Nevertheless, some transcription factors linked to neural progenitor fates show differential expression in the neural plate[9,33,35–38]. This suggests that patterning begins in the neural plate,

and could be regulated by the signals active in this context. The extent of such neural plate "pre-patterning" and its impacts on downstream neural progenitor specification in the neural tube is unclear.

Here, we undertook a systematic analysis of the zebrafish neural plate, combining measurements of signaling activity, expression of transcription factors (TFs), and morphogenetic movements. We found extensive spatial patterning by TFs, which partition the tissue into distinct states in response to signals present during gastrulation and axis extension. Indeed, signaling perturbations combined with analysis of cell movements and fate-mapping showed that Wnt signaling in this region helps establish the boundary between future dorsal and ventral neural progenitor domains. Importantly, it also defines a transient TF state at this boundary that prefigures the p0 progenitor cell fate in the intermediate neural tube. Thus, in addition to signaling gradients in the neural tube, dorso-ventral patterning in the spinal cord relies on pre-patterning of the neural plate by Wnt signaling.

Results

Mapping differential transcription factor expression in the neural plate

To characterize the neural plate systematically, we first developed a reference-based mapping approach to enable comparisons between spatial measurements made in stage-matched embryos (Methods). The neural plate in zebrafish embryos could be identified as a *sox19a*-positive region posterior to the first somite (Figure 1A, B). For reference-mapping, measurements were made in double transgenic embryos in which the notochord and cell boundaries are fluorescently labeled using a *shha:GFP* reporter and a ubiquitous membrane-localized mNeonGreen protein, respectively (Figure S1A, B). Based on these signals, new coordinates were calculated for each cell: its medio-lateral distance from the midline and antero-posterior distance from the end of the extending notochord, both calculated along the surface of the embryo, and its depth from the surface (Figure 1C). Unlike imaging coordinates, these coordinates should be robust to changes in the orientation of the embryo because they are contained within the frame of reference of the embryo. We verified that reference-mapped expression patterns for a previously identified neural plate gene, *olig4*[37] remained relatively constant despite changes in the orientation of imaging (Figure S1C, D).

We next sought to characterize regulatory cell states in the neural plate by analyzing the expression of heterogeneous transcription factors (TFs). We analyzed single-cell transcriptomic data from 10 hpf (hours post fertilization) zebrafish embryos[39], identifying TFs in the posterior neural tissue that are highly variable between cells, expressed above a threshold value, and non-redundant (Methods). This analysis returned 28 TFs. We supplemented this list with three marker genes for intermediate spinal cord fates (*dbx1b, prdm12b,* and *irx3a*), two of which were detected in the analysis as being highly variable but did not cross the expression threshold.

We then used dual-color HCR RNA-FISH to measure the expression of each of these genes along with *sox19a* as a neural marker[40]. We chose to make these measurements in 5-6 ss embryos; at this stage, the neural plate is 1-cell thick in most regions (Figure S1B), and could be treated as a pseudo-two dimensional tissue, simplifying subsequent analyses. Mapping the location of cells

using the photoconvertible fluorescent protein KikGR showed that the neural plate at this stage contributes to the majority of the neural tube (somites 9-27) (Figure S1E) presumably due to convergence-extension movements during axis elongation. We could detect expression of 22 TFs within the neural plate. Other genes were either expressed primarily in non-neural regions (*tfap2a, nr2f5*) or in the tailbud (*cdx1a)*, or were detected at very low levels, consistent with their low expression in previous *in situ* analyses (ZFIN) as well as a recent spatial transcriptomic dataset (Methods)[41].

Expression of detected neural plate TFs was then reference-mapped, revealing diverse spatial expression patterns (Figure 1D, Figure S2A-D). Expression of most TFs was enriched in particular sub-regions of the plate, but together their expression covered the entire neural plate, indicating that our TF selection procedure captures spatial heterogeneity across the neural plate. Each expression pattern was unique, indicating diverse upstream regulation and elaborate positional information at the neural plate stage. Importantly, reference maps could be used to reliably estimate TF co-expression: comparing the *in silico* overlays for selected pairs of genes with co-expression based on dual-color HCR-FISH showed that reference mapping could capture both co-expression and exclusion along both the medio-lateral (ML) and antero-posterior (AP) axes (Figure 1E, Figure S2E).

These maps revealed that markers for different neural progenitor fates emerge at different A-P levels. Future ventral markers such as *olig2, nkx6.1/6.2* show posterior expression near the medial line, while more intermediate markers such as *pax6b, irx3a, prdm12b* and *dbx1b* emerge at progressively more anterior levels (Figure S3A). Some broad markers of dorsal fates such as *pax3a* and *olig4* are expressed in posterior regions, but others such as *ascl1b* are not detected in the neural plate (Figure S3B). Moreover, *her3* is strongly expressed in the plate but not the tube (Figure S3C). Thus, the neural plate represents a distinct state of the neural tissue compared to the neural tube.

Together, these data show that the neural plate is richly patterned by TFs and that reference-based maps of these spatial patterns can be used to infer co-expression states of TFs.

The neural plate is organized into multiple TF co-expression states

Next, we sought to characterize regulatory states in the neural plate by systematically analyzing TF co-expression. We first smoothed the reference maps by agglomerating pixels into approximately cell-sized ‘superpixels’, which we then subsequently analyzed using principal component analysis (PCA) and k-means clustering (Figure 2A, Methods).

Visualizing the weights of superpixels along the first six principal components (capturing ~90% of gene expression variance) revealed major modes of neural plate organization: broad divisions into 3 or 4 domains along the ML and AP axes (component 1 and components 2 and 3, respectively) as well as more refined divisions along both axes (components 4-6) (Figure 2B-C, Figure S4A-D). Clustering superpixels based on gene expression (Methods, Figure S4E) and visualizing the location of cluster labels in the neural plate similarly revealed a grid-like

organization, suggesting that cells throughout the plate possess information about their relative AP/ML position (Figure 2D, E).

Notably, even the posterior region of the plate, which does not contribute to the neural tube until the end of somitogenesis (Figure S1E), is subdivided into multiple distinct clusters (#13-16) along the ML axis. These are characterized both by transient TFs confined to the neural plate, such as *her3* (Figure S4C), as well as TFs that persist until the neural tube, such as *pax3a*, *olig2* and *nkx6.2*. Moreover, the presence of multiple clusters along the AP axis, between these posterior clusters and those in the anterior of the neural plate, suggests that cells transit through intermediate states as they progress through the neural plate *en route* to the neural tube.

To infer possible relationships between the TF states represented by these clusters, we analyzed their gene expression similarity (Methods). Clusters were generally more similar to AP neighbors compared to ML neighbors, indicating that state transitions likely occur in this direction (Figure 2F). In particular, clusters near the midline (4, 7, 8, 12, 15, 16 and 3, 6, 11) are closely related (top 1/3 of gene expression similarity). Potential transitions from posterior to anterior appear to be characterized by early expression of ventral neural progenitor TFs such as *olig2, nkx6.1, nkx6.2,* and *prdm8a,* followed by expression of *irx3a* and *pax6b* (more laterally) and *neurog1, her6 and her15.1* (more medially). This is consistent with previous suggestions that the neural tissue displays increasing specification from posterior to anterior[14].

Clusters at the lateral margin (1, 9, 13) are also closely related, marked by the expression of *pax3a* and *zic2a* posteriorly, and more anterior expression of *olig4, neurog1, her6* and *pax6b.* The close similarity within the medial and lateral clusters suggested that, by exclusion, clusters in intermediate ML positions (2, 5, 10, 14) could be linked developmentally. However, their gene expression similarity is lower on average, indicating that TF expression changes more substantially among these states.

We note that the averaging of multiple embryos to generate the reference map and the subsequent downsampling for clustering analysis blurs local heterogeneity in gene expression, such as in the case of “salt and pepper” expression of *neurog1*. This analysis therefore likely underestimates the extent of spatial patterning in the neural plate. Nevertheless, it captures broad differences in TF co-expression in different regions of the neural plate. Together, these results showed that the entire neural plate is partitioned into multiple regulatory states marked by distinct combinations of TFs, and raises the question of how this pre-pattern affects cell neural tube patterning.

Ventral neural progenitor fates emerge from a pre-patterned her3+ *region*

We next sought to better understand the relationships between cells in the intermediate neural plate, located in clusters that have relatively low similarity to their neighbors. Notably, markers for p0 and p1 neural progenitors, *dbx1b* and *prdm12b* respectively, first appear in the anterior of this region (cluster 2 in Figure 2D, E).

We monitored the neural plate between 2ss to 6ss using timelapse imaging of a nuclear-localized H2B-mScarlet fluorescent protein controlled by the *sox19a* promoter (Figure 3A, Methods). These embryos also expressed the notochord reporter (*shha:GFP*). Following automated tracking analysis, cell nuclei could therefore be reference-mapped at each time point to generate a map of relative cell motion in the neural plate (Figure 3A-C, Figure S5A). This analysis confirmed that, as the axis elongates, cells move anteriorly relative to the extending notochord end, while converging towards the midline.

To link these movements to TF expression states in the intermediate neural plate, we next analyzed them in relation to the expression domain of *her3*, which covers a large portion of this region and largely defines it (for e.g., it contributes most to principal component 2 in Figure 2B-C). Comparing the change in *her3* expression between 4ss and 6ss to directions of cell motion between these developmental time points suggested that the movement of cells shifts the lateral-posterior boundary of *her3* toward the middle (Figure 3D). However, the medial-anterior boundary does not shift substantially despite the flow of cells towards it, indicating that it marks a transition in cell state from *her3*+ to *her3-.* What do these cells become when they lose *her3* expression? Examination of the reference-maps of genes that display a sharp change across this boundary suggested that anteriorly, *her3* cells produce *dbx1b*+ and *prdm12b*+ cells, while more posteriorly, they produce *olig2*+ and *nkx6.1*+ cells (Figure 3E-F, Figure S5B). Indeed, dual-color HCR-FISH showed cells at the boundary that co-express *her3* and each of these potential derivative genes, likely corresponding to cells in transition (Figure 3G-H, Figure S5C-E).

To directly track the fate of her3 cells, we also analyzed a long-lived mScarlet-NLS fluorescent reporter regulated by a 4.7kb *her3* promoter[32] (Methods). This reporter accurately reflects the lateral boundary of her3 expression in the neural plate (Figure S5F), which corresponds to the future dorsal extent (in the neural tube) of cells derived from this region. We found that in the neural tube, cells at the dorsal extent of the *her3* reporter co-expressed a *dbx1b*:*GFP* reporter[42], (Figure 3I). This confirms the origin of *dbx1b*+ p0 progenitors from the *her3*+ region in the neural plate and further indicates that these cells emerge from the lateral edge of *her3*.

Thus, ventral progenitor fates, from *dbx1b*+ p0 cells to *olig2*+ pMN cells, appear to emerge from a pre-patterned *her3*+ region in the neural plate. The lateral boundary of *her3* in the neural plate thus corresponds to the boundary between future dorsal and ventral neural tube fates. We note that, consistent with this, the *her3* reporter does not colocalize with *pax3a* or *olig4* in the neural tube (Figure S5G, H). Together, these analyses show that the neural plate is subdivided from an early stage into prospective dorsal and ventral regions. In particular, *dbx1b*+ p0-fated cells emerge from the lateral boundary of the *her3* domain, while more ventral fates (p1-pMN) emerge from more medial positions within this region.

dbx1b *cells originate from a region of transient co-expression of* her3 *and* pax3a/olig4

We next asked what, if anything, was distinct about the lateral boundary of *her3* that biased cells in this region towards the *dbx1b*+ fate. Examining TF expression clusters indicated that cells in this region specifically co-express *olig4* (Cluster 10 in Figure 2E), which could be verified using dual color HCR-FISH for *olig4* and *her3* (Figure 4A, B). We note that *pax3a* and *olig4* show

correlated expression in this region, suggesting that *her3*, *olig4* and *pax3a* are co-expressed along the lateral boundary of *her3* (Figure S6A).

This distinct co-expression state raised the possibility that this *olig4/pax3a/her3* subpopulation of cells produces *dbx1b*+ cells. Interestingly, however, we found that *olig4* and *dbx1b* are not co-expressed (Figure S6B). To ask whether this reflected transient expression of *olig4/pax3a* within *dbx1b* precursor cells, we sought to analyze the fate of cells in this region. Using a previously described GFP reporter for pax3a (tgBAC(*pax3a:GFP*))[43] we indeed observed co-expression between *GFP* expression and *dbx1b* (Figure 4C).

Together, these data support a model in which *dbx1b*+ cells derive from a sub-region of the *her3* domain that transiently co-expresses the lateral genes *pax3a* and *olig4*. We note that an origin for *dbx1b* from *pax3a*+ cells is also consistent with previous *Pax3* fate-mapping results in mouse[44,45].

Wnt signaling defines olig4/her3 *co-expression and promotes* dbx1b *specification*

To understand how the *olig4/pax3a* + *her3* co-expression domain in the neural plate is determined, we next analyzed signaling in the neural plate. Previous work has suggested that ligands for five pathways – FGF, Wnt, Notch, Shh, and BMP - are expressed in the neural plate and tailbud region[31,33,46,47]. We systematically analyzed the activity of these pathways using either HCR RNA-FISH for known target genes (Wnt, Notch, Shh) or immunofluorescence to detect phosphorylated pathway effectors (FGF, BMP). As with transcription factor analyses (Figure 1), these measurements were made along with HCR RNA-FISH for the neural marker *sox19a* in *shha:GFP* transgenic embryos, enabling reference mapping.

We found that there was no discernible BMP activity (phosphoryated-Smad1/5/8 immunofluorescence) in the neural plate (Figure S6C), but the other pathways show patterned activity in the neural plate (Figure 4D). In particular, in addition to Shh signaling along the midline, we observed the Wnt target *sp5l* (Figure S6D)[46] in the medial-posterior regions, the Notch target *her4.2* in the anterior medial and lateral regions, and a posterior to anterior gradient of the FGF target phospho-ERK. Interestingly, the activity region of each signaling pathway was generally congruent with particular TF clusters, suggesting that neural plate TF expression is defined by these signals (Figure 4E, Figure S6E).

In particular, comparing *sp5l* with TF clusters indicated that it defines the boundary of cluster 10, which marks the *her3/olig4* state (Figure 4E). A direct comparison of *sp5l* and *olig4* indicated that they have largely complementary expression domains, but that the two genes are co-expressed at their boundary, which we confirmed using dual color HCR-FISH (Figure 4F, G). Their complementarity suggested that Wnt signaling might restrict the medial extent of *olig4.* Consistent with this, inhibiting Wnt signaling (Methods) led to medial encroachment of *olig4* (Figure 4H-I, S6F), shifting the *her3/olig4* co-expression region (Figure S6H). We note that expansion of *olig4* occurs in its posterior region, where it normally abuts *sp5l*, but not in more anterior regions. This indicates that other genes likely maintain the *olig4* boundary anteriorly. We also note that Wnt inhibition did not significantly affect *pax3a* expression (Figure S6G). Thus, Wnt signaling in the

posterior neural plate specifically helps define the boundary of *olig4* and its co-expression with *her3*.

Notably, the region of co-expression between *sp5l* and *olig4* also overlaps with the *dbx1b* precursor region (*her3+/olig4+*) (Figure 4J). Based on this, we hypothesized that Wnt signaling within the *olig4* region could play a role in *dbx1b* specification. To test this, we mosaically expressed a constitutively-active form of β-catenin ('CA-βCat-tagBFP2') in double transgenic embryos expressing *dbx1b:GFP* as well as *her3:mScarlet-NLS*, which was used to label the ventral half of neural tube (Figure 2I). We found that expression of CA-bCat-tagBFP2, but not a tagBFP2 control, led to ectopic GFP+ cells dorsal to the mScarlet-NLS domain (Figure 4K-L, Figure S6I). This suggests conversion of *pax3a* and *olig4* cells, which normally occupy the dorsal neural tube (Figure S4G-H), to *dbx1b*.

Together, these data suggest a model in which Wnt signaling in the posterior-medial region of the neural plate functions to both define the *her3/olig4* co-expression region by limiting the *olig4* domain and to induce cells in this region toward becoming *dbx1b+* cells.

Discussion

Understanding how cells in developing tissues become specified in a spatiotemporally controlled manner is a fundamental goal in developmental biology. Here, we showed that pre-patterning in the neural plate plays a critical role in dorsal-ventral cell fate specification in the neural tube. A systematic analysis of transcription factor expression (Figure 1, 2) and signaling activity (Figure 4) demonstrated that the neural plate shows substantial patterning. Co-expression of patterned TFs partitions the tissue into distinct states along the medio-lateral and antero-posterior axes. Broadly, these reflect early subdivisions of the tissue into future dorsal, intermediate and ventral regions, which are progressively elaborated as cells transition from neural plate to neural tube. Importantly, patterns of signaling activity in the neural plate can explain TF states and transitions. In particular, p0 neural progenitors, characterized by *dbx1b* expression, arise from a neural plate-specific state characterized by transient co-expression of TFs (Figure 3) and Wnt activity (Figure 4).

Pre-patterning the tissue to specify cell fate in the intermediate neural tube represents a distinct patterning strategy compared to the Shh and BMP gradient-based mechanisms that have been shown to be important for patterning ventral[48,49] and dorsal[18,19,50] fates, respectively. Interestingly, while activity of Shh is evident in the medial neural plate and corresponds to expression of ventral fate markers such as *olig2* and *nkx6.1/6.2* (Figure 4D, Figure 1D), BMP activity is not discernible in most of the neural plate, consistent with recent work in mouse embryos[14]. Nevertheless, the lateral neural plate is patterned by TFs like *pax3a, olig4, zic2a/b* and *neurog1* (Figure 1D, clusters 1 and 5 in Figure 2D, E). This suggests that neural plate patterning could also impact dorsal fate specification in the neural tube, possibly contributing to observations that dorsal cells display distinct BMP preferences in this context[20,27]. In general, it is likely that tissue pre-patterning and gradient-based mechanisms work together to generate the fine-grained array of cell fates in the neural tube. We find that the pre-pattern is itself organized by neural plate-specific Wnt signaling,

arguing for a model in which the final D-V pattern is achieved through successive exposure to different signals at different stages, which progressively refine cell states.

Specifically, Wnt activity in the early neural plate helps establish the future dorsal vs. ventral boundary (by limiting *olig4*) and defining prospective *dbx1b* cells at this boundary (Figure 4G-K). This is distinct from the mitogenic role of Wnts emanating from the roof plate which has been shown in amniotes[51,52]. We note that Wnt activity has also been implicated in regulating neighboring tissues such as the tailbud and mesoderm. Wnt perturbation thus leads to broad effects on anterior-posterior regionalization[30], axis elongation[46] and mesoderm development [53,54], possibly explaining why its role in neural plate patterning has been overlooked.

Here we show how that *dbx1b*+ cells specifically emerge from a transient *her3/olig4/pax3a* co-expressing region that is defined by Wnt signaling. Importantly, expression of *dbx1b* is not initiated until the mRNA levels of all of these factors are diminished (Figure S6B, Figure 3G-H), though their protein levels may endure longer. Future work will address the molecular mechanisms by which transient expression of these factors and Wnt signaling promotes downstream *dbx1b* expression. Our results are consistent with previous analysis of *dbx1b* expression in zebrafish that show that its expression does not require Shh signaling[22,23].

More broadly, we observe differential and non-redundant activity of multiple signaling pathways, including FGF and Notch, across the neural plate (Figure 3C). Comparing their spatial activity domains to TF expression states suggests that, like Wnt, they also impact neural plate patterning (Figure S6E). The diversification and organization of cell fates in the neural tube thus likely reflects the coordinated spatiotemporal actions of multiple signals acting during gastrulation and axis extension. Our systematic analysis of signaling and TFs complements recent sequencing-based efforts to characterize cell fate lineages in an unbiased manner[52,55]. These represent important steps towards an integrated view of this system that will clarify the basis of neural fate specification, open up new therapeutic avenues for programming fate, and inform efforts to understand the developmental patterning of other tissues.

Acknowledgements

The authors thank members of the Megason and Lahav labs for helpful feedback. S.N. was the Philip O'Bryan Montgomery, Jr., MD, Fellow of the Damon Runyon Cancer Research Foundation (DRG-2339-18) and is supported by National Institute of Health grant 1K99GM151398. Research in the Megason Lab is supported by National Institutes of Health grant R01GM107733.

Author Contributions

S.N, A.C and S.G.M designed experiments. S.N, A.C, B.Z.J, H.L and C.C performed experiments. D.E.W and T.Y-C.T generated key reagents and transgenic lines. S.N and S.G.M wrote the manuscript with input from all authors.

Figure 1

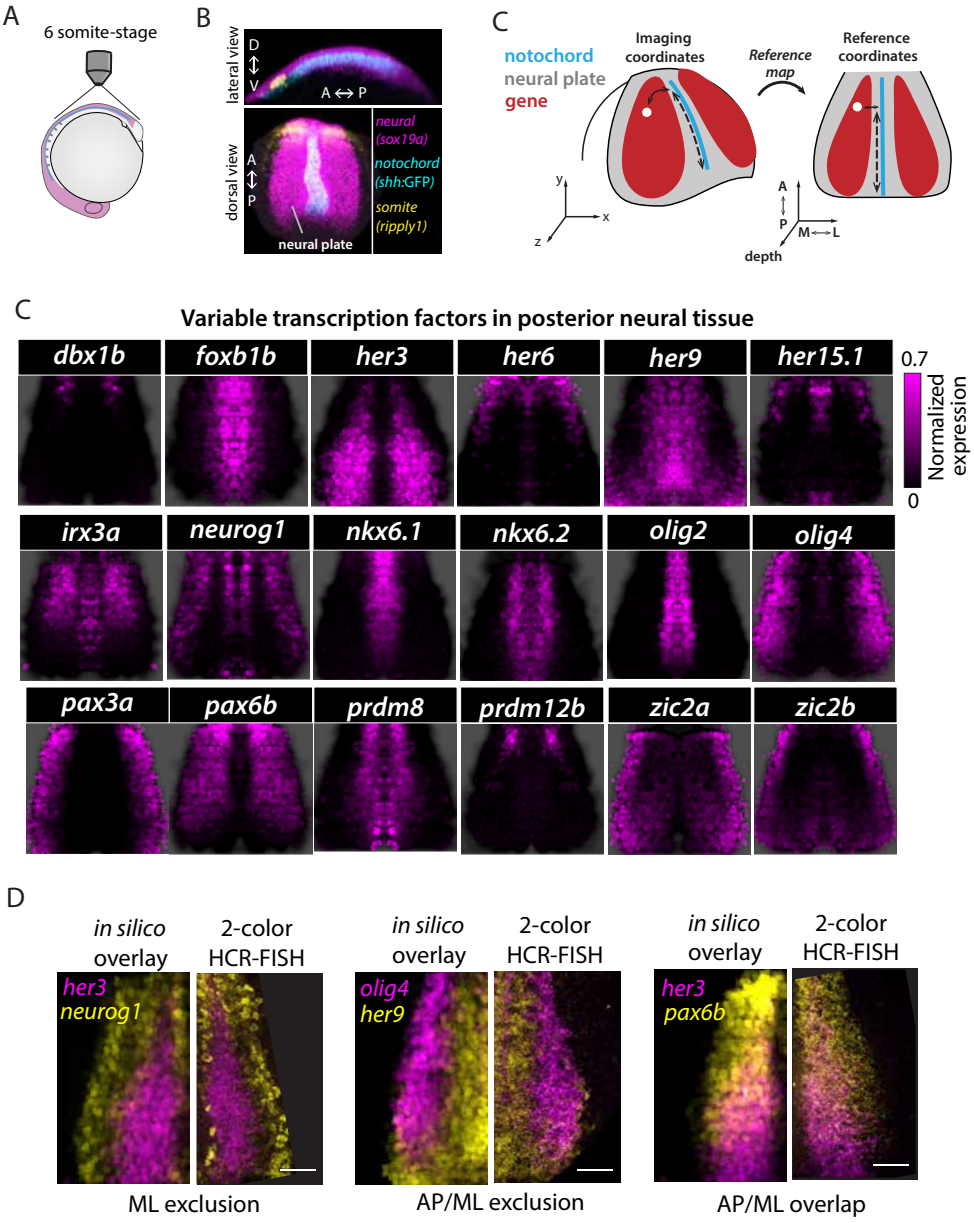

Figure 1. **The neural plate shows patterned expression of several transcription factors, which can be compared *in silico* after reference-mapping.**

(A) Schematic showing approximate orientation of 5-6 somite-stage (ss) zebrafish embryo used for imaging the neural plate.

(B) 3D-rendered visualization of 5-6 ss embryo expressing *shh:GFP* (cyan), with HCR RNA-FISH labeling of sox19a (magenta) and ripply1 (yellow) expression, and imaged as in (A). Lateral and dorsal views are shown. “A” = Anterior; “P” = Posterior. “D” = Dorsal; “V” = Ventral.

(C)Schematic showing reference-mapping transformation from imaging coordinates to reference-based coordinates. “M” = Medial; “L” = Lateral.

(D) Reference-maps showing mRNA expression (magenta) of the indicated transcription factors, measured using HCR RNA-FISH. The black background corresponds to the neural plate, co-labeled in each measurement using *sox19a*. Each map depicts the average of reference-mapped HCR RNA-FISH signal across n = 3 embryos, each symmetrized and normalized to the maximal detected signal within the image. See also Figure S1C, S2A-D.

(E) Comparison between *in silico* overlays of the reference-maps for the indicated genes (left half of each split panel) and representative examples of their co-expression within a single embryo (right half of each split panel, maximum intensity projection), measured using two-color HCR RNA-FISH. Scale bar indicates 50 μm.

Figure 2

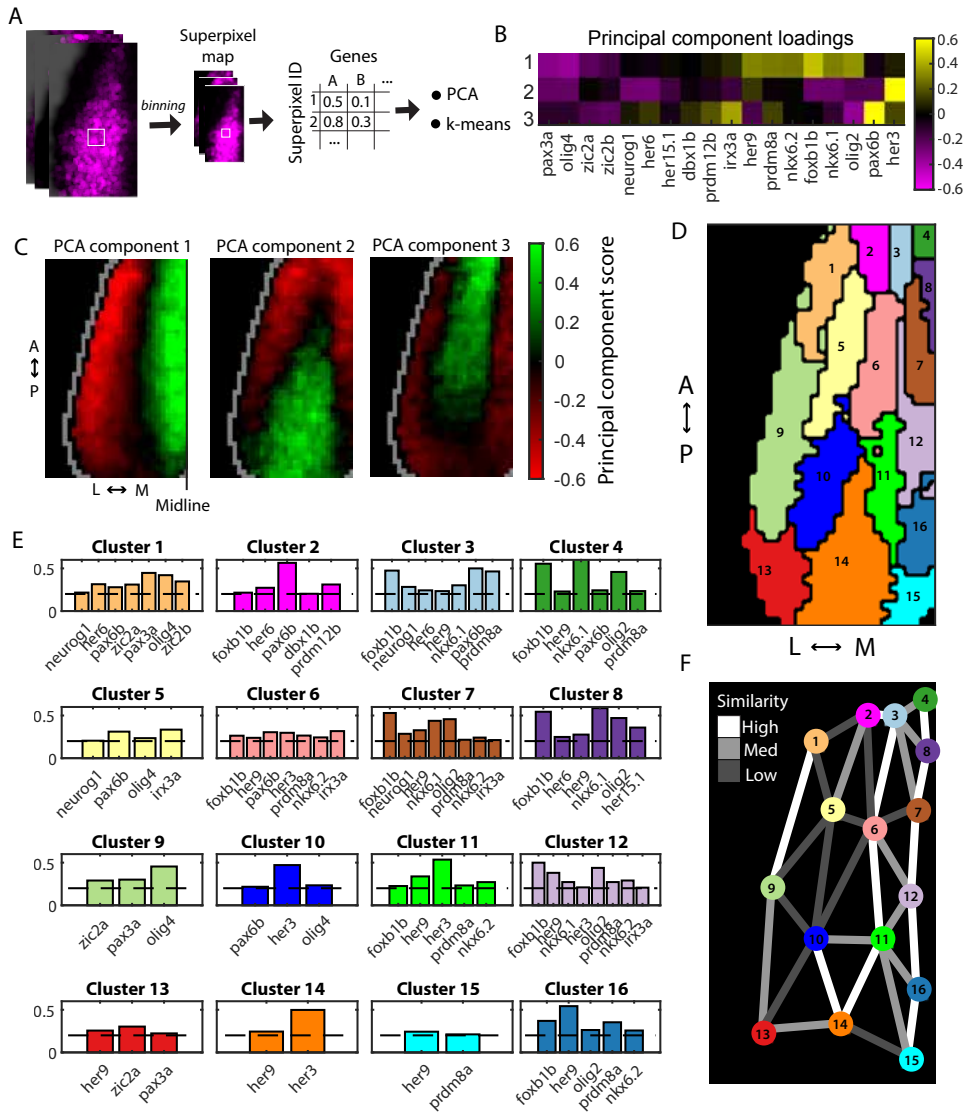

Figure 2. **The neural plate is partitioned into multiple TF co-expression states.**

(A) Schematic of analysis workflow. Each TF reference-map was first downsampled through binning of pixels to generate a corresponding map of 'superpixels'. Superpixels were then analyzed by principal component analysis (PCA) and *k*-means clustering.

(B) Loading values per TF (columns) for each of the first three principal components (rows). Higher absolute values indicate a greater contribution of a TF towards the corresponding principal component. See also Figure S4C.

(C) Map of superpixel weights along the first three principal components. See also Figure S4B.

(D) Map of cluster labels for superpixels after *k*-means clustering.

(E) Mean expression levels of indicated TFs within the individual clusters shown in (D). Only TFs with mean expression above a threshold (dashed line) are shown.

(F) Similarity between clusters, measured by distance in gene-expression values. 'High' similarity indicates that the distance between corresponding clusters is in the lowest 33rd percentile of all pairwise distances between clusters, 'Medium' similarity indicates distance in the 33rd - 66th percentile, and 'Low' indicates distance is >66th percentile. Note that links are only shown between clusters that share a boundary.

Figure 3

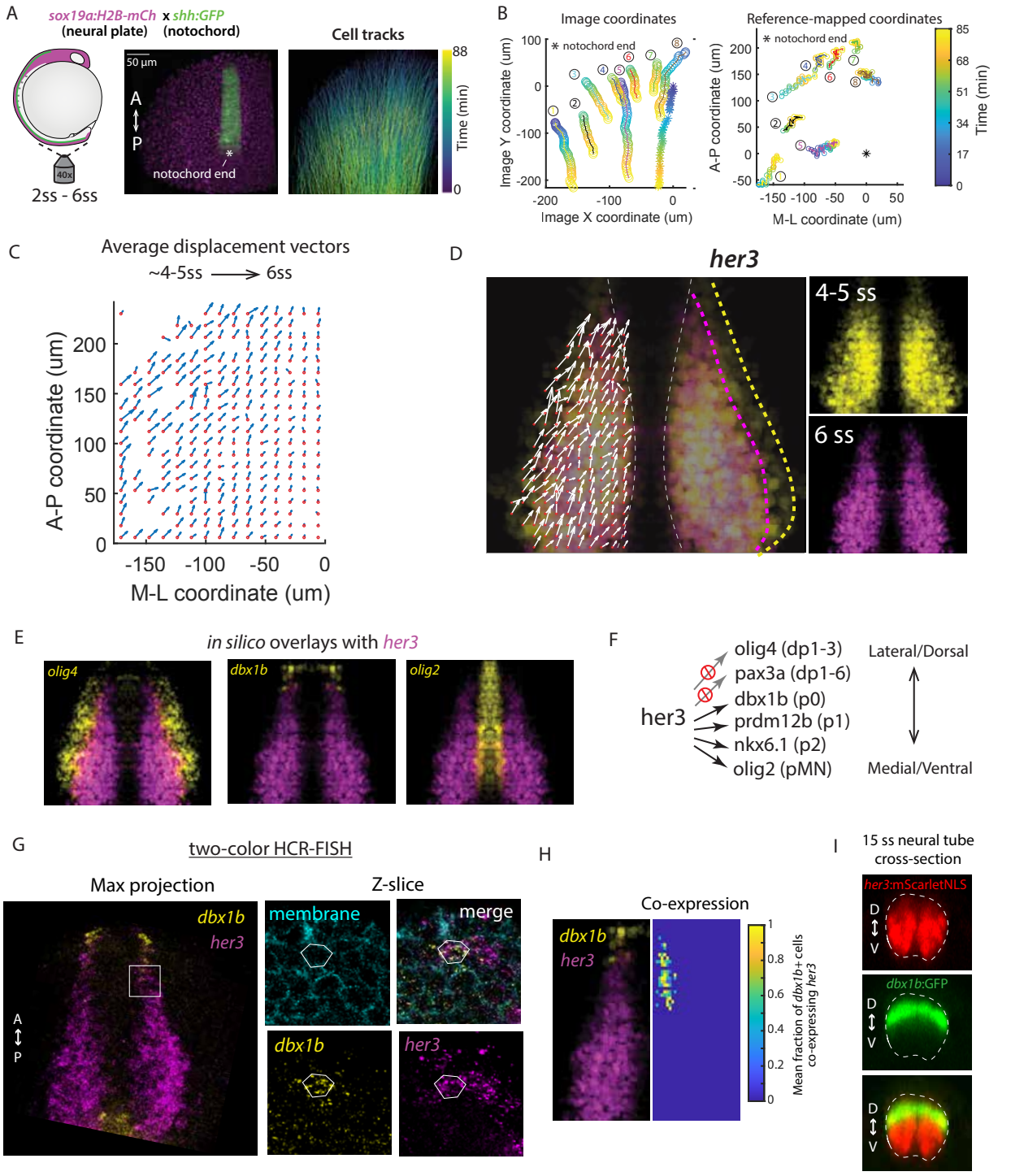

Figure 3. ***dbx1b*+ cells emerge from the lateral boundary of *her3* expression in the neural plate.**

(A) (*Left*) Schematic showing region of *sox19a*:H2B-mCherry, *shh*:GFP double-transgenic embryo that was imaged to analyze cell movement in the neural plate. (*Middle*) 3D-rendered visualization of imaged area at 4 ss. Asterisk indicates the approximate position of the posterior tip of the notochord, annotated manually. "A" = Anterior; "P" = Posterior. (*Right*) Cell tracks indicating the position of cells at different timepoints during timelapse imaging.

(B) Position over time for selected cells (#1-8) and the notochord end point (asterisk), in image coordinates (*left*) and after reference-mapping relative to the reference point (*right*).

(C) Mean reference-mapped displacement vectors (blue arrows) for cells in the neighborhood of the indicated positions (orange markers) between 4-5s ss and 6 ss (20 min time period). Displacement vectors from corresponding positions on the left and right sides of the embryo have been averaged. See Figure S5A for (non-averaged) displacement on left and right sides.

(D) Overlay of displacement vectors from (C) and reference-mapped expression of *her3* at 4-5 ss (yellow) and 6 ss (magenta). Yellow and magenta colored dashed lines indicate lateral boundaries of *her3* expression at 4-5 ss and 6 ss, respectively. White dashed line indicate medial boundary. Note that vectors outside *her3* expression regions are not shown.

(E) *in silico* overlays of reference-maps for the indicated genes; same data as Figure 1C.

(F) Schematic showing that ventral fates, but not dorsal fates, emerge from the her3 region in the neural plate.

(G) (*Left*) Representative example of *her3* (magenta) and *dbx1b* (yellow) expression, measured using HCR RNA-FISH, in a single embryo that expresses a membrane-localized mNeongreen fluorescent protein (not shown). Maximum projection of 3D image is shown. (*Right*) A single Z-slice of the 3D image showing membrane fluorescence (cyan). An individual cell co-expressing *her3* (magenta) and *dbx1b* (yellow) expression is outlined.

(H) (*Left*) *in silico* overlay of *dbx1b* (yellow) and *her3* (magenta) reference-maps; same data as Figure 1C. (*Right*) Heat map showing average fraction of *dbx1b*+ cells that co-express *her3* within n = 3 individual embryos in which both genes are labeled using HCR RNA-FISH.

(I) Cross-section of 15 ss neural tube in double transgenic embryos expressing *her3*:mScarlet-NLS (red) and TgBAC(*dbx1b*:GFP) (green). The dashed line indicates the region of the neural tube expressing mScarlet-NLS.

Figure 4

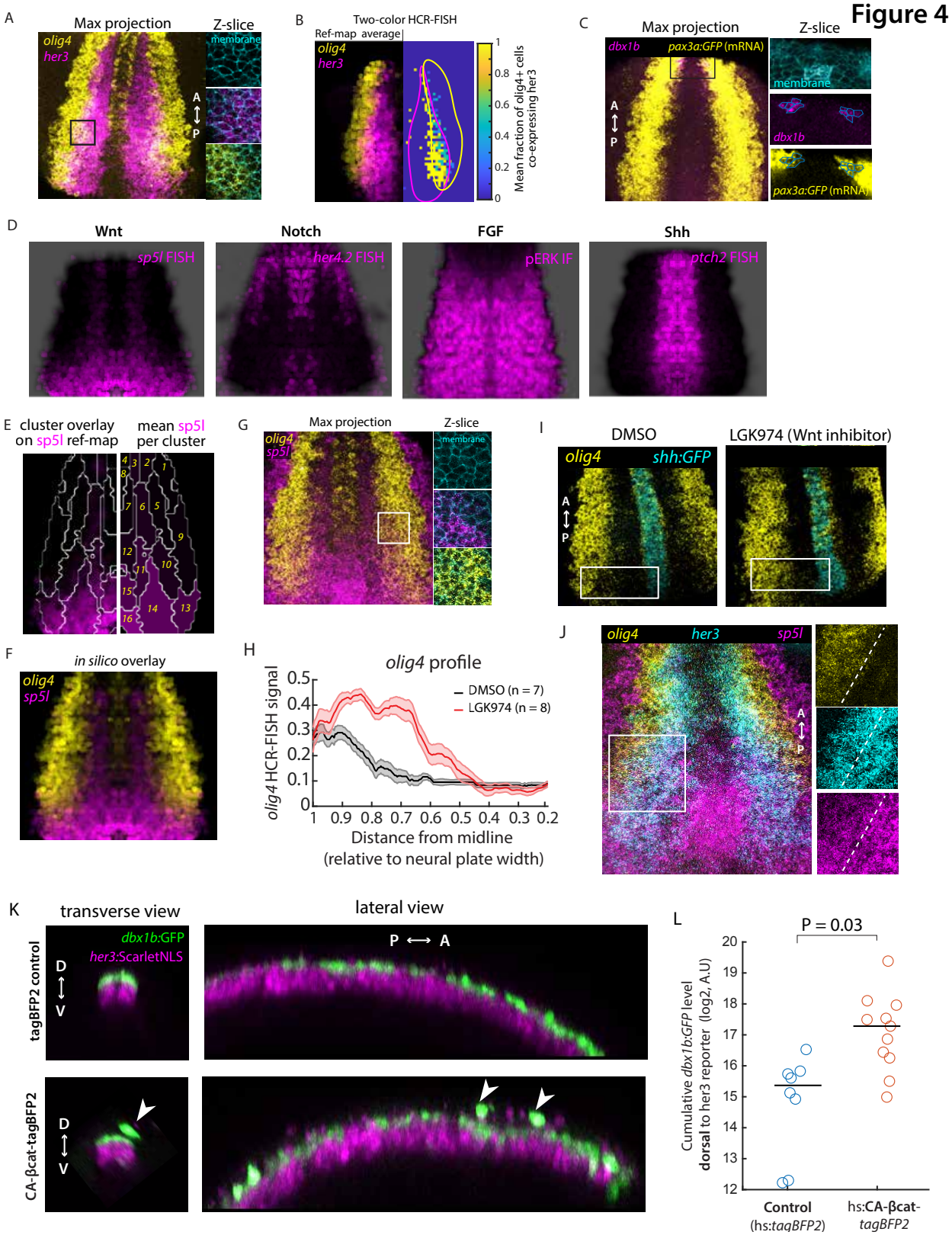

Figure 4. **Neural plate Wnt signaling determines *dbx1b* precursor region.**

(A) (*Left*) Representative example of *her3* (magenta) and *olig4* (yellow) expression, measured using HCR RNA-FISH, in a single embryo that expresses a membrane-localized mNeongreen fluorescent protein (not shown). Maximum projection of 3D image is shown. (*Right*) A single Z-slice of region outlined in black showing membrane fluorescence (cyan) (top panel), overlaid with *her3* (middle panel) or *olig4* (bottom panel).

(B) (*Left*) Average reference-mapped expression of *olig4* (yellow) and *her3* (magenta) (n = 2 embryos). (*Right*) Heat map showing average fraction of *olig4*+ cells that co-express *her3* within individual embryos in which both genes are labeled using HCR RNA-FISH.

(C) (*Left*) Representative example of *dbx1b* (magenta) and *GFP* mRNA (yellow) expression, measured using HCR RNA-FISH, in a TgBAC(*pax3a:GFP*) transgenic embryo that also expresses a membrane-localized mNeongreen fluorescent protein (not shown). Maximum projection of 3D image is shown. (*Right*) A single Z-slice of the 3D image showing membrane fluorescence (cyan) (top panel), overlaid with *dbx1b* (middle panel) or *GFP* (bottom panel). Individual cells co-expressing *dbx1b* (magenta) and *GFP* (yellow) expression are outlined.

(D) Reference-maps of indicated signaling pathway targets. Each map depicts the average of reference-mapped signal across n = 3 embryos, each symmetrized and normalized to the maximal detected signal within the image.

(E) (*Left*) Outlines of TF clusters overlaid on average *sp5l* reference-map (magenta, same as 4D). (*Right*) Mean reference-mapped *sp5l* expression within TF clusters (labels as in Figure 2D, E).

(F) *in silico* overlay of *olig4* (yellow) and *sp5l* (magenta) reference-maps; same data as Figure 1C, 4D.

(G) (*Left*) Representative example of *sp5l* (magenta) and *olig4* (yellow) expression, measured using HCR RNA-FISH, within an individual embryo that also expresses a membrane-localized mNeongreen fluorescent protein (not shown). Maximum projection of 3D image is shown. (*Right*) A single Z-slice of the 3D image showing membrane fluorescence (cyan) (top panel), overlaid with *sp5l* (middle panel) or *olig4* (bottom panel). Note co-expression of *sp5l* and *olig4* in individual cells.

(H-I) *olig4* response to Wnt inhibition. (H) Representative examples of *olig4* (yellow) expression, measured using HCR RNA-FISH, after treatment with LGK974 (*right*) or DMSO control (*left*). Embryos express a *shh*:GFP reporter (cyan). Maximum projection of 3D image is shown. White boxes indicate regions used to calculate medio-lateral profile of *olig4* in (I). (I) Median medio-lateral profile of *olig4* in embryos treated with LGK974 (red) or DMSO control (black). Shaded regions indicates S.E.M. n indicates number of embryos.

(J) (*Left*) Representative example of *sp5l* (magenta), *olig4* (yellow) and *her3* (cyan) expression, measured using HCR RNA-FISH, within an individual embryo. Maximum projection of 3D image is shown. (*Right*) A single Z-slice of region outlined in white showing co-expression of *sp5l* and *her3* with *olig4*; dashed line indicates medial boundary of *olig4*.

(K-L) *dbx1b:GFP* response to Wnt activation. (K) Representative examples of transverse (left column) and sagittal (right column) cross-sections of 15-18 ss neural tube after mosaic expression of CA-βcat-tagBFP2 (bottom) or tagBFP2 control (top) in transgenic embryos expressing *her3*:mScarlet-NLS (magenta) and TgBAC(*dbx1b*:GFP) (green). (L) Cumulative *dbx1b:GFP* signal dorsal to *her3:mScarlet-NLS* reporter. Circles represent different embryos, while horizontal line indicates median. *P* value calculated using Student's T-Test. See also Figure S6I.

Methods

Zebrafish strains

Zebrafish (*Danio rerio*) were raised, maintained, and used for experiments as per protocols approved by the Harvard Medical Area Institutional Animal Care and Use Committee (HMA IACUC). AB and TL strain fish were used for all experiments. Juveniles and adults were maintained on a 14 h light / 10 h dark cycle at ~28°C. Embryos were typically obtained from 4 mo – 18 mo old fish, and raised at 25 to 33°C.

The following new transgenic lines were generated for this study and are described below: Tg(*sox19a:H2B-mCherry2*) and Tg(*her3:mScarlet-NLS*). The following transgenic strains were also used and have been described previously: TgBAC(*dbx1b:GFP*)^{nn11} [56], TgBAC(*pax3a:GFP*)^{i130} [43], Tg(*shha:GFP*)[57], Tg(*actb2:MA-2xmNeongreen*)^{hm40}.

Generation of transgenic lines

Tg(sox19a:H2B-mScarlet): An amplicon spanning a ~6.7kb genomic sequence upstream of the predicted sox19a translation start site was PCR-amplified from a chromosome 5 BAC clone (CH73-378C22, CHORI-BACPAC) using primers 5-GCATAATCTAGCGCGAGTCC-3 and 5-CATGGCTGCCAACAGAAGT-3, Phusion polymerase, and the following cycling parameters: 98°C for 1 min, 35 cycles of 98°C for 10 sec, 64°C for 30 sec, and 72°C for 3 min, followed by 72°C for 5 min and a 4°C hold. The resulting amplicon was ligated into a pMTB vector backbone fragment (AddGene #112225) amplified with the same cycling parameters and primers 5-ACTTCTGTTGGCAGCCATGTCTAAAGGTGAAGAACTGTTCA-3 and 5-GGACTCGCGCTAGATTATGCGTAATGACTAGGCCCTCGAGC-3 by isothermal assembly to replace the original actb2 promoter with that of sox19a. Subsequently, reporter downstream of the promoter was replaced with an mScarlet gene fused to histone 2B (H2B).

Tg(her3:Scarlet-NLS): A ~4.7 kb fragment of the *her3* promoter[32] was amplified from a pBSceI-her3:GalTA plasmid [58] and cloned upstream of an mScarlet gene fused to an SV40 NLS sequence (PKKKRKV).

Transgenic founders were identified following the co-microinjection of single-cell stage zebrafish embryos with Tol2 mRNA and the resulting plasmid DNA.

Confocal Microscopy

All imaging was performed on a Zeiss LSM980 laser scanning confocal microscope using a Plan-Apochromat 20X 1.0 NA, C-Apochromat 40X/1.1 NA, or a LD LCI Plan-Apochromat 40x/1.2 NA objective. A ~300 µm x 300 µm x 100 µm region was imaged in a typical experiment.

For timelapse imaging, embryos were maintained at 25-28 C in egg water and mounted using a previously described procedure[9] that allowed long-term imaging of the posterior neural plate.

For imaging of fixed embryos, particularly for samples used to generate transcription factor and signaling activity maps, they were mounted in PDMS casts (10% cross-linker, with 1% Triton-X100) and embedded in Prolong Gold Antifade Mountant (ThermoFisher) prior to imaging using the LD LCI Plan-Apochromat 40x/1.2 NA immersed in glycerol.

Reference-mapping

For reference-mapping, measurements were typically made in transgenic embryos in which cells are fluorescently labeled, either using a ubiquitously expressed membrane-or nuclear-localized fluorescent protein, and the notochord is fluorescently labeled using a *shha:GFP* reporter. Following confocal imaging, membrane-labeled cells were individually segmented using PlantSeg [59], while nuclear-labeled cells were identified in Imaris (v10.0). Custom MATLAB software was used to manually annotate the approximate dorsal midline of the notochord and to automatically calculate the outer surface of the embryo based on standard thresholding-based analysis.

Next, the sagittal plane of the embryo was calculated by using the anterior, posterior, and dorsal extrema of the annotated notochord midline. A mediolateral coordinate was assigned to each segmented cell/nucleus based on its distance from the sagittal plane, calculated along contours defined by the shape of the embryo surface. An anteroposterior coordinate was similarly calculated, based on the distance from the posterior tip of the annotated midline. Finally, the depth of the cell was calculated based on its distance from the embryo surface, along the normal vector to the surface. These three coordinates constitute the 'reference-based' coordinates for each cell.

To construct the reference-map for a given measurement, segments were translated to their reference-based coordinates within a new 3D image, with all pixel values within each segment assigned its mean signal value.

Selection of transcription factors for neural plate characterization from single-cell data

Cells from 10 hpf within a previously-described transcriptomic dataset covering different stages of zebrafish embryogenesis[39] were analyzed to identify potential spatially patterned transcription factors in the neural plate. Using SCANPY[60], cells annotated as 'posterior neural tissue' were isolated, organized into 10 Louvain clusters, and the 'highly-variable' function was used to identify the 200-most overdispersed genes. These genes were then cross-referenced with annotated zebrafish transcription factors (AnimalTFdb 4.0[61]) to identify variable transcription factors (TFs). Next, TFs expressed above a maximum value of 0.3 within at least one Louvain cluster were identified. Next, correlated genes were identified: for each pair of genes, their cross-correlation of mean expression across clusters was calculated, and genes were hierarchically clustered based on this. For sets of genes with median cross-correlation above a threshold value, only the highest expressed member was retained. This procedure yielded 28 TFs for further analysis.

The following TFs showed very low or undetectable HCR RNA-FISH signal within the neural plate and were not used further: *fosab, hnf1ba, junbb, meis3, pax6a,* and *id2a*.

Identification of TF co-expression states and similarity

Reference-maps were generated as 3D images at approximately the resolution of the original confocal image (0.5 um x 0.5 um x 0.7 um) but transformed into 2D by maximum projection along the depth axis. These maps were subsequently downsampled for analysis by binning pixels 10x10 (corresponding approximately to the size of a cell in the neural plate, 5 um diameter). For analysis of TF variation and clustering, the map for each gene was transformed into a vector by concatenating rows in the image matrix. Principal Component Analysis and k-means clustering were performed on these map vectors.

For calculation of gene expression similarity, each cluster was analyzed as a vector in an 18-dimensional space, with dimensions corresponding to the 18 different genes displayed in Figure 2C and its value along each gene dimension corresponding to the mean expression of that gene within the cluster. Similarity was assessed using a cosine similarity distance.

Chemical perturbation of Wnt signaling

LGK974 (SelleckChem, Catalog No.S7143) was stored at a stock concentration of 10 mM in DMSO. For perturbation experiments, bud-stage (10 hpf) embryos were dechorionated using Pronase (2 mg/ml) and then treated with 10 uM LGK974 (0.5% final concentration of DMSO) in Danieau buffer. Treated embryos were raised at 28 C for 3h, and subsequently washed 3 times with Danieau buffer prior to fixation.

References

1. Briscoe, J., and Small, S. (2015). Morphogen rules: design principles of gradient-mediated embryo patterning. Development *142*, 3996–4009. https://doi.org/10.1242/dev.129452.
2. Tuazon, F.B., and Mullins, M.C. (2015). Temporally coordinated signals progressively pattern the anteroposterior and dorsoventral body axes. Semin. Cell Dev. Biol. *42*, 118–133. https://doi.org/10.1016/j.semcdb.2015.06.003.
3. Sjöqvist, M., and Andersson, E.R. (2019). Do as I say, Not(ch) as I do: Lateral control of cell fate. Dev. Biol. *447*, 58–70. https://doi.org/10.1016/j.ydbio.2017.09.032.
4. Landge, A.N., Jordan, B.M., Diego, X., and Müller, P. (2020). Pattern formation mechanisms of self-organizing reaction-diffusion systems. Dev. Biol. *460*, 2–11. https://doi.org/10.1016/j.ydbio.2019.10.031.
5. Huang, A., and Saunders, T.E. (2020). A matter of time: Formation and interpretation of the Bicoid morphogen gradient. Curr. Top. Dev. Biol. *137*, 79–117. https://doi.org/10.1016/bs.ctdb.2019.11.016.
6. Kicheva, A., Bollenbach, T., Ribeiro, A., Valle, H.P., Lovell-Badge, R., Episkopou, V., and Briscoe, J. (2014). Coordination of progenitor specification and growth in mouse and chick spinal cord. Science *345*, 1254927. https://doi.org/10.1126/science.1254927.

7. Jaeger, J., Irons, D., and Monk, N. (2008). Regulative feedback in pattern formation: towards a general relativistic theory of positional information. Development *135*, 3175–3183. https://doi.org/10.1242/dev.018697.
8. Spiess, K., Taylor, S.E., Fulton, T., Toh, K., Saunders, D., Hwang, S., Wang, Y., Paige, B., Steventon, B., and Verd, B. (2024). Approximated gene expression trajectories for gene regulatory network inference on cell tracks. iScience *27*, 110840. https://doi.org/10.1016/j.isci.2024.110840.
9. Xiong, F., Tentner, A.R., Huang, P., Gelas, A., Mosaliganti, K.R., Souhait, L., Rannou, N., Swinburne, I.A., Obholzer, N.D., Cowgill, P.D., et al. (2013). Specified neural progenitors sort to form sharp domains after noisy Shh signaling. Cell *153*, 550–561. https://doi.org/10.1016/j.cell.2013.03.023.
10. Xiong, F., Tentner, A.R., Nandagopal, S., Hiscock, T.W., Huang, P., and Megason, S.G. (2024). Heterogeneity of Sonic Hedgehog response dynamics and fate specification in single neural progenitors. https://doi.org/10.7554/elife.96980.
11. Tsai, T.Y.-C., Sikora, M., Xia, P., Colak-Champollion, T., Knaut, H., Heisenberg, C.-P., and Megason, S.G. (2020). An adhesion code ensures robust pattern formation during tissue morphogenesis. Science *370*, 113–116. https://doi.org/10.1126/science.aba6637.
12. Camacho-Aguilar, E., Yoon, S.T., Ortiz-Salazar, M.A., Du, S., Guerra, M.C., and Warmflash, A. (2024). Combinatorial interpretation of BMP and WNT controls the decision between primitive streak and extraembryonic fates. Cell Syst. *15*, 445-461.e4. https://doi.org/10.1016/j.cels.2024.04.001.
13. Teague, S., Primavera, G., Chen, B., Liu, Z.-Y., Yao, L., Freeburne, E., Khan, H., Jo, K., Johnson, C., and Heemskerk, I. (2024). Time-integrated BMP signaling determines fate in a stem cell model for early human development. Nat. Commun. *15*, 1471. https://doi.org/10.1038/s41467-024-45719-9.
14. Lehr, S., Brückner, D.B., Minchington, T.G., Greunz-Schindler, M., Merrin, J., Hannezo, E., and Kicheva, A. (2024). Self-organized pattern formation in the developing mouse neural tube by a temporal relay of BMP signaling. Dev. Cell. https://doi.org/10.1016/j.devcel.2024.10.024.
15. Purvis, J.E., and Lahav, G. (2013). Encoding and decoding cellular information through signaling dynamics. Cell *152*, 945–956. https://doi.org/10.1016/j.cell.2013.02.005.
16. Nandagopal, N., Santat, L.A., LeBon, L., Sprinzak, D., Bronner, M.E., and Elowitz, M.B. (2018). Dynamic Ligand Discrimination in the Notch Signaling Pathway. Cell *172*, 869-880.e19. https://doi.org/10.1016/j.cell.2018.01.002.
17. Moon, L.D., and Xiong, F. (2022). Mechanics of neural tube morphogenesis. Semin. Cell Dev. Biol. *130*, 56–69. https://doi.org/10.1016/j.semcdb.2021.09.009.
18. Wine-Lee, L., Ahn, K.J., Richardson, R.D., Mishina, Y., Lyons, K.M., and Crenshaw, E.B., 3rd (2004). Signaling through BMP type 1 receptors is required for development of interneuron cell types in the dorsal spinal cord. Development *131*, 5393–5403. https://doi.org/10.1242/dev.01379.
19. Müller, T., Anlag, K., Wildner, H., Britsch, S., Treier, M., and Birchmeier, C. (2005). The bHLH factor Olig3 coordinates the specification of dorsal neurons in the spinal cord. Genes Dev. *19*, 733–743. https://doi.org/10.1101/gad.326105.

20. Andrews, M.G., Del Castillo, L.M., Ochoa-Bolton, E., Yamauchi, K., Smogorzewski, J., and Butler, S.J. (2017). BMPs direct sensory interneuron identity in the developing spinal cord using signal-specific not morphogenic activities. Elife *6*. https://doi.org/10.7554/eLife.30647.
21. Timmer, J.R., Wang, C., and Niswander, L. (2002). BMP signaling patterns the dorsal and intermediate neural tube via regulation of homeobox and helix-loop-helix transcription factors. Development *129*, 2459–2472.
22. Gribble, S.L., Nikolaus, O.B., and Dorsky, R.I. (2007). Regulation and function of Dbx genes in the zebrafish spinal cord. Dev. Dyn. *236*, 3472–3483. https://doi.org/10.1002/dvdy.21367.
23. England, S., Batista, M.F., Mich, J.K., Chen, J.K., and Lewis, K.E. (2011). Roles of Hedgehog pathway components and retinoic acid signalling in specifying zebrafish ventral spinal cord neurons. Development *138*, 5121–5134. https://doi.org/10.1242/dev.066159.
24. Zannino, D.A., Downes, G.B., and Sagerström, C.G. (2014). prdm12b specifies the p1 progenitor domain and reveals a role for V1 interneurons in swim movements. Dev. Biol. *390*, 247–260. https://doi.org/10.1016/j.ydbio.2014.02.025.
25. Wijgerde, M., McMahon, J.A., Rule, M., and McMahon, A.P. (2002). A direct requirement for Hedgehog signaling for normal specification of all ventral progenitor domains in the presumptive mammalian spinal cord. Genes Dev. *16*, 2849–2864. https://doi.org/10.1101/gad.1025702.
26. Litingtung, Y., and Chiang, C. (2000). Specification of ventral neuron types is mediated by an antagonistic interaction between Shh and Gli3. Nat. Neurosci. *3*, 979–985. https://doi.org/10.1038/79916.
27. Andrews, M.G., Kong, J., Novitch, B.G., and Butler, S.J. (2019). New perspectives on the mechanisms establishing the dorsal-ventral axis of the spinal cord. Curr. Top. Dev. Biol. *132*, 417–450. https://doi.org/10.1016/bs.ctdb.2018.12.010.
28. Diez del Corral, R., and Storey, K.G. (2004). Opposing FGF and retinoid pathways: a signalling switch that controls differentiation and patterning onset in the extending vertebrate body axis. Bioessays *26*, 857–869. https://doi.org/10.1002/bies.20080.
29. Deschamps, J., and van Nes, J. (2005). Developmental regulation of the Hox genes during axial morphogenesis in the mouse. Development *132*, 2931–2942. https://doi.org/10.1242/dev.01897.
30. Metzis, V., Steinhauser, S., Pakanavicius, E., Gouti, M., Stamataki, D., Ivanovitch, K., Watson, T., Rayon, T., Mousavy Gharavy, S.N., Lovell-Badge, R., et al. (2018). Nervous system regionalization entails axial allocation before neural differentiation. Cell *175*, 1105-1118.e17. https://doi.org/10.1016/j.cell.2018.09.040.
31. Cornell, R.A., and Eisen, J.S. (2000). Delta signaling mediates segregation of neural crest and spinal sensory neurons from zebrafish lateral neural plate. Development *127*, 2873–2882. https://doi.org/10.1242/dev.127.13.2873.
32. Hans, S., Scheer, N., Riedl, I., Weizsäcker, E., v, Blader, P., and Campos-Ortega, J.A. (2004). her3, a zebrafish member of the hairy-E(spl) family, is repressed by Notch signalling. Development *131*, 2957–2969. https://doi.org/10.1242/dev.01167.
33. Diez del Corral, R., Olivera-Martinez, I., Goriely, A., Gale, E., Maden, M., and Storey, K. (2003). Opposing FGF and retinoid pathways control ventral neural pattern, neuronal differentiation, and segmentation during body axis extension. Neuron *40*, 65–79. https://doi.org/10.1016/s0896-6273(03)00565-8.

34. Sasai, N., Kutejova, E., and Briscoe, J. (2014). Integration of signals along orthogonal axes of the vertebrate neural tube controls progenitor competence and increases cell diversity. PLoS Biol. *12*, e1001907. https://doi.org/10.1371/journal.pbio.1001907.
35. Bae, Y.-K., Shimizu, T., and Hibi, M. (2005). Patterning of proneuronal and inter-proneuronal domains by hairy- and enhancer of split-related genes in zebrafish neuroectoderm. Development *132*, 1375–1385. https://doi.org/10.1242/dev.01710.
36. Bang, A.G., Papalopulu, N., Goulding, M.D., and Kintner, C. (1999). Expression of Pax-3 in the lateral neural plate is dependent on a Wnt-mediated signal from posterior nonaxial mesoderm. Dev. Biol. *212*, 366–380. https://doi.org/10.1006/dbio.1999.9319.
37. Filippi, A., Tiso, N., Deflorian, G., Zecchin, E., Bortolussi, M., and Argenton, F. (2005). The basic helix-loop-helix olig3 establishes the neural plate boundary of the trunk and is necessary for development of the dorsal spinal cord. Proc. Natl. Acad. Sci. U. S. A. *102*, 4377–4382. https://doi.org/10.1073/pnas.0407284102.
38. Henrique, D., Tyler, D., Kintner, C., Heath, J.K., Lewis, J.H., Ish-Horowicz, D., and Storey, K.G. (1997). cash4, a novel achaete-scute homolog induced by Hensen's node during generation of the posterior nervous system. Genes Dev. *11*, 603–615. https://doi.org/10.1101/gad.11.5.603.
39. Wagner, D.E., Weinreb, C., Collins, Z.M., Briggs, J.A., Megason, S.G., and Klein, A.M. (2018). Single-cell mapping of gene expression landscapes and lineage in the zebrafish embryo. Science *360*, 981–987. https://doi.org/10.1126/science.aar4362.
40. Choi, H.M.T., Schwarzkopf, M., Fornace, M.E., Acharya, A., Artavanis, G., Stegmaier, J., Cunha, A., and Pierce, N.A. (2018). Third-generation in situ hybridization chain reaction: multiplexed, quantitative, sensitive, versatile, robust. Development *145*. https://doi.org/10.1242/dev.165753.
41. Wan, Y., El Kholtei, J., Jenie, I., Colomer-Rosell, M., Liu, J., Acedo, J.N., Du, L.Y., Codina-Tobias, M., Wang, M., Sawh, A., et al. (2024). Whole-embryo Spatial Transcriptomics at Subcellular Resolution from Gastrulation to Organogenesis. bioRxiv. https://doi.org/10.1101/2024.08.27.609868.
42. Satou, C., Kimura, Y., Hirata, H., Suster, M.L., Kawakami, K., and Higashijima, S.-I. (2013). Transgenic tools to characterize neuronal properties of discrete populations of zebrafish neurons. Development *140*, 3927–3931. https://doi.org/10.1242/dev.099531.
43. Seger, C., Hargrave, M., Wang, X., Chai, R.J., Elworthy, S., and Ingham, P.W. (2011). Analysis of Pax7 expressing myogenic cells in zebrafish muscle development, injury, and models of disease. Dev. Dyn. *240*, 2440–2451. https://doi.org/10.1002/dvdy.22745.
44. Gard, C., Gonzalez Curto, G., Frarma, Y.E.-M., Chollet, E., Duval, N., Auzié, V., Auradé, F., Vigier, L., Relaix, F., Pierani, A., et al. (2017). Pax3- and Pax7-mediated Dbx1 regulation orchestrates the patterning of intermediate spinal interneurons. Dev. Biol. *432*, 24–33. https://doi.org/10.1016/j.ydbio.2017.06.014.
45. Moore, S., Ribes, V., Terriente, J., Wilkinson, D., Relaix, F., and Briscoe, J. (2013). Distinct regulatory mechanisms act to establish and maintain Pax3 expression in the developing neural tube. PLoS Genet. *9*, e1003811. https://doi.org/10.1371/journal.pgen.1003811.
46. Thorpe, C.J., Weidinger, G., and Moon, R.T. (2005). Wnt/beta-catenin regulation of the Sp1-related transcription factor sp5l promotes tail development in zebrafish. Development *132*, 1763–1772. https://doi.org/10.1242/dev.01733.

47. Esterberg, R., Delalande, J.-M., and Fritz, A. (2008). Tailbud-derived Bmp4 drives proliferation and inhibits maturation of zebrafish chordamesoderm. Dev. Biol. *319*, 580. https://doi.org/10.1016/j.ydbio.2008.05.401.
48. Balaskas, N., Ribeiro, A., Panovska, J., Dessaud, E., Sasai, N., Page, K.M., Briscoe, J., and Ribes, V. (2012). Gene regulatory logic for reading the Sonic Hedgehog signaling gradient in the vertebrate neural tube. Cell *148*, 273–284. https://doi.org/10.1016/j.cell.2011.10.047.
49. Sagner, A., and Briscoe, J. (2019). Establishing neuronal diversity in the spinal cord: a time and a place. Development *146*. https://doi.org/10.1242/dev.182154.
50. Tozer, S., Le Dréau, G., Marti, E., and Briscoe, J. (2013). Temporal control of BMP signalling determines neuronal subtype identity in the dorsal neural tube. Development *140*, 1467–1474. https://doi.org/10.1242/dev.090118.
51. Megason, S.G., and McMahon, A.P. (2002). A mitogen gradient of dorsal midline Wnts organizes growth in the CNS. Development *129*, 2087–2098. https://doi.org/10.1242/dev.129.9.2087.
52. Gupta, S., Kawaguchi, R., Heinrichs, E., Gallardo, S., Castellanos, S., Mandric, I., Novitch, B.G., and Butler, S.J. (2022). In vitro atlas of dorsal spinal interneurons reveals Wnt signaling as a critical regulator of progenitor expansion. Cell Rep. *40*, 111119. https://doi.org/10.1016/j.celrep.2022.111119.
53. Aulehla, A., Wehrle, C., Brand-Saberi, B., Kemler, R., Gossler, A., Kanzler, B., and Herrmann, B.G. (2003). Wnt3a plays a major role in the segmentation clock controlling somitogenesis. Dev. Cell *4*, 395–406. https://doi.org/10.1016/s1534-5807(03)00055-8.
54. Blassberg, R., Patel, H., Watson, T., Gouti, M., Metzis, V., Delás, M.J., and Briscoe, J. (2022). Sox2 levels regulate the chromatin occupancy of WNT mediators in epiblast progenitors responsible for vertebrate body formation. Nat. Cell Biol. *24*, 633–644. https://doi.org/10.1038/s41556-022-00910-2.
55. Delile, J., Rayon, T., Melchionda, M., Edwards, A., Briscoe, J., and Sagner, A. (2019). Single cell transcriptomics reveals spatial and temporal dynamics of gene expression in the developing mouse spinal cord. Development *146*, dev173807. https://doi.org/10.1242/dev.173807.
56. Kinkhabwala, A., Riley, M., Koyama, M., Monen, J., Satou, C., Kimura, Y., Higashijima, S.-I., and Fetcho, J. (2011). A structural and functional ground plan for neurons in the hindbrain of zebrafish. Proc. Natl. Acad. Sci. U. S. A. *108*, 1164–1169. https://doi.org/10.1073/pnas.1012185108.
57. Shkumatava, A., Fischer, S., Müller, F., Strahle, U., and Neumann, C.J. (2004). Sonic hedgehog, secreted by amacrine cells, acts as a short-range signal to direct differentiation and lamination in the zebrafish retina. Development *131*, 3849–3858. https://doi.org/10.1242/dev.01247.
58. Babaryka, A., Kühn, E., and Köster, R.W. (2009). In vivo synthesis of meganuclease for generating transgenic zebrafish Danio rerio. J. Fish Biol. *74*, 452–457. https://doi.org/10.1111/j.1095-8649.2008.02075.x.
59. Wolny, A., Cerrone, L., Vijayan, A., Tofanelli, R., Barro, A.V., Louveaux, M., Wenzl, C., Strauss, S., Wilson-Sánchez, D., Lymbouridou, R., et al. (2020). Accurate and versatile 3D segmentation of plant tissues at cellular resolution. Elife *9*. https://doi.org/10.7554/eLife.57613.

60. Wolf, F.A., Angerer, P., and Theis, F.J. (2018). SCANPY: large-scale single-cell gene expression data analysis. Genome Biol. *19*. https://doi.org/10.1186/s13059-017-1382-0.
61. Shen, W.-K., Chen, S.-Y., Gan, Z.-Q., Zhang, Y.-Z., Yue, T., Chen, M.-M., Xue, Y., Hu, H., and Guo, A.-Y. (2023). AnimalTFDB 4.0: a comprehensive animal transcription factor database updated with variation and expression annotations. Nucleic Acids Res. *51*, D39–D45. https://doi.org/10.1093/nar/gkac907.